MICROENDOSCOPIC CALCIUM IMAGING IN SUPPLEMENTARY MOTOR AREA AND PRIMARY MOTOR CORTEX OF RHESUS MACAQUES AT REST AND DURING ARM MOVEMENT

Anne-Caroline Martel[*1,2,6], Damien Pittard*[1,2,6], Annaelle Devergnas[1,3,6], Benjamin Risk[2,4,6], Jonathan J. Nassi[5,6], Waylin Yu[5], Joshua D. Downer[5], Thomas Wichmann[1,2,3,6], Adriana Galvan[1,2,3,6]

(*both authors contributed equally to this work)

[1]Emory National Primate Research Center, [2]Udall Center of Excellence for Parkinson's Disease Research, [3]Dept of Neurology (School of Medicine), [4]Dept of Biostatistics & Bioinformatics (Rollins School of Public Health), Emory University, Atlanta, GA, USA
[5]Inscopix Inc., Mountain View, CA, USA
[6]Aligning Science Across Parkinson's (ASAP) Collaborative Research Network, Chevy Chase, MD, 20815

Corresponding author: Anne-Caroline Martel, amarte4@emory.edu

HIGHLIGHTS

- Use of one-photon miniature microscopes and microendoscopic calcium imaging to study the activity of cortical projection neurons in the supplementary motor area (SMA) and primary motor cortex (M1) of rhesus macaques at rest or performing simple arm reaches.
- Calcium transients were related to arm reaches and showed directional sensitivity in a proportion of cells in SMA and M1.
- Subsets of cell pairs showed coactivation in SMA and M1 during rest and reaching tasks. The strength of coactivity was not related to the distance between cells.
- SMA and M1 neurons displayed sequential activation patterns.
- We demonstrated that microendoscopic calcium imaging can be used to assess dynamic activity within genetically identified cell populations in deep layers of SMA and M1.

SUMMARY

The study of motor cortices in non-human primates is relevant to our understanding of human motor control, both in healthy conditions and in movement disorders. Calcium imaging and miniature microscopes allow the study of multiple genetically identified neurons with excellent spatial resolution. We used this method to examine activity patterns of projection neurons in deep layers of the supplementary motor (SMA) and primary motor areas (M1) in four rhesus macaques. We implanted gradient index lenses and expressed GCaMP6f to image calcium transients while the animals were at rest or engaged in an arm reaching task. We tracked the activity of SMA and M1 neurons across conditions, examined cell pairs for synchronous activity, and assessed whether SMA and M1 neuronal activation followed specific sequential activation patterns. We demonstrate the value of *in vivo* calcium imaging for studying patterns of activity in groups of corticofugal neurons in SMA and M1.

KEYWORDS

One-photon calcium imaging, non-human primates, microendoscope, reaching task, neuronal coactivation, calcium sensors, GCaMP, GRIN lens

INTRODUCTION

Cortical motor regions have undergone significant evolutionary expansion, specialization, and re-organization (Strick et al., 2021), therefore non-human primates (NHPs) are often used to model motor control in humans under healthy conditions, and during movement disorders such as Parkinson's disease. In primates, the motor cortices include the primary motor cortex (M1) and the supplementary motor area (SMA) (Nachev et al., 2008; Picard and Strick, 1996), which are components of larger frontal networks that also involve portions of the basal ganglia and the ventral anterior and ventral lateral thalamus (Alexander and Crutcher, 1990; Alexander et al., 1986; McFarland and Haber, 2001; Middleton and Strick, 2000). Neurons in M1 and SMA are involved in movement planning and execution (Nachev et al., 2008; Tanji and Mushiake, 1996).

The majority of studies on cortical neuronal activity in awake NHPs have used extracellular electrophysiological recordings. Methods such as one-photon fluorescent miniature microscope (miniscope) imaging of genetically-encoded calcium indicators offer an alternative approach to monitor neuronal activity, and have recently been used to study calcium transients in individual cells in the

premotor and visual cortices of macaques (Bollimunta et al., 2021; Oguchi et al., 2021; Pollmann et al., 2023).

When combined with microendoscopic gradient index (GRIN) lenses, miniscopes enable optical access to non-superficial imaging regions, and allow prolonged monitoring of multiple individual neurons in the brain region of interest, providing detailed understanding of spatial relationships among cells. Calcium indicators, such as GCaMP, can be genetically directed to be expressed in selective cell populations, and the resulting calcium activities of identified neurons can be followed throughout the course of an experiment, enabling tracking of the same cells across behavioral conditions (e.g., from rest to active movement).

We used microendoscopic calcium imaging to examine the activity of neuronal ensembles in SMA and M1 in four rhesus macaques while the monkeys were at rest or performing simple arm reaches. Following expression of the genetically encoded calcium indicator GCaMP6f in projection neurons of deep cortical layers of SMA and M1, we tracked the activity of these neurons across conditions, examined cell pairs for synchronous activity or inactivity, and assessed whether neuronal activation followed specific sequential activation patterns. Our results demonstrate that calcium imaging captures dynamic activity patterns in SMA and M1 neurons and establish a basis for future research on how SMA and M1 activities change during the development of parkinsonism and other disorders of movement in NHPs.

METHODS

The key resources used in this study (including plasmids, viral vectors, and antibodies along with citations to the protocols used) are listed in supplementary table 3 (Table S3)

Animals

Four rhesus macaques (Macaca mulatta) were studied (monkeys F, Q, U, and V, 2 males, 2 females). The animals were 4 - 5 years old and weighed 5.5 - 6.8 kg at the beginning of the study. The monkeys were pair-housed in a temperature-controlled room with a 12-hour light cycle, fed a standard primate diet twice daily with additional fruit and vegetable supplements, and had access to water *ad libitum*. All procedures were approved by the Institutional Animal Care and Use Committee (IACUC) of Emory University and were performed according to the Guide for the Care and Use of Laboratory Animals and the U.S. Public Health Service Policy on the Humane Care and Use of Laboratory Animals.

Behavioral task

Two of the monkeys (Q and U) were first trained to accept head fixation with a thermoplastic molded helmet (CIVCO medical solutions) (Drucker et al., 2015) or a surgically implanted head post, and then trained on an arm reaching task (NIMH, MonkeyLogic v2.2). The monkeys were facing a 17-inch display touchscreen (GVision) during task performance. Training began 2-4 weeks before lens implant surgery (see below) and continued until the animals reached criteria (see below).

Monkey Q was trained in a one-target task that required the animal to touch a circle (~93mm diameter) shown on the touchscreen display with his right hand to receive a juice reward. For each trial, the target would randomly appear on the right, left, or center of the touchscreen and remained illuminated for up to 3s. If the monkey touched it during this period (successful trials), the target disappeared, and the animal received a drop of juice. A new trial started after a random inter-trial interval (2-3 s), following the release of the monkey's hand from the touchscreen.

Monkey U was trained in a two-target task, in which the monkey had to first touch a center target (circle, ~52 mm diameter) with its right hand for the imaging sessions evaluating the left SMA, or with his left hand for the imaging sessions focused on the right M1. After the monkey had held the center target for 1 s, targets on the left or right side of the screen (randomly chosen) would appear. The monkey had to release the center target within 1s and touch the side target (successful trial), to receive a drop of juice.

We considered monkeys trained in these tasks when they consistently completed at least 100 successful trials per 10-minute session.

Surgery (AAV injections and lens implant)

Monkeys were subjected to a surgery to receive injection of virus solutions and implantation of GRIN lenses, following previously described methods (see Table S3 and (Bollimunta et al., 2021)). The location of the lens implants was determined based on pre-surgery MRI scans and stereotaxic coordinates obtained from (Paxinos et al., 2000). The surgery was performed under sterile conditions. Monkeys were sedated with ketamine (10mg/kg), followed by isoflurane anesthesia (1-3%) for the remainder of the procedure. They were placed in a stereotactic frame, and their vital signs were monitored throughout the surgical procedure.

We performed two craniotomies, each producing skull defects measuring approximately 10 mm in diameter, over the arm regions of the left SMA and the right M1. Following the craniotomies, we made a small incision in the dura mater for virus injections and GRIN lens implants at each cortical site.

We used a virus solution consisting of a 1:1 mixture of AAV5-TRE-GCAMP6f (9.05x10e13 gc/ml) and AAV5-ThyStTA (5.13x10e13 gc/ml). The Tet-Off system strategy was used because the GCaMP6f expression is amplified due to the tetracycline (tTA) promoter activation of the tetracycline response element (TRE3) (Bollimunta et al., 2021; Kondo et al., 2018). In addition, if needed, GCaMP6f expression could be temporarily suppressed with systemic administration of doxycycline (Bollimunta et al., 2021). Note, however, that doxycycline was not used in these studies. A Hamilton syringe with a 25-ga needle was filled with the mixture and then lowered into the brain using an injection pump mounted to the stereotactic frame (Stoelting quintessential stereotaxic injector). We started injections of the virus solution after a three-minute wait time.

We injected 3-6.4 and 5-7.8 µl (at 0.1 – 0.8µl/min) of virus solution in M1 and SMA, respectively. Information about the depths and volumes of injections in each site are provided in supplementary table 2. The needle remained at each injection site for at least 3 min after the final injection.

After the virus injection, an epoxy-filled 18-ga needle was lowered into the brain to create a path for the subsequent insertion of a GRIN prism for M1 (1 mm diameter, 9 mm, or 12 mm length), or a flat lens for SMA (1 mm diameter, 12 mm length), pre-attached to a baseplate to dock a miniscope (ProView Integrated Probe or ProView Integrated Prism Probe; Inscopix). The baseplate with the integrated lenses were lowered into the brain to target the center of the dorsal-ventral extent of the virus injections. Following the lens implantation, a cranial chamber was positioned around each baseplate-integrated lens, affixed to the skull, and capped for protection. The exposed brain tissue around the lens was covered with gel foam and a slotted aluminum disk. The implant was secured to the disk and skull within the chamber with Metabond dental cement (Parkell, Edgewood, NY) or Gradia Direct Flo light-cured composite (GC Corp., Tokyo Japan). Finally, the exposed skull was covered with bone screws and dental acrylic. We then secured a head holder in the dental acrylic cap.

Calcium imaging data acquisition

Nineteen to 48 days post-surgery, we started imaging calcium transients in SMA and M1 neurons using a head-mounted miniscope (nVista3.0, Inscopix, CA, USA). The miniscope was docked to the integrated baseplate of the implanted lenses. Imaging data for each site were acquired at least twice weekly. During these sessions, the monkeys were sitting on a primate chair and remained awake (confirmed by continuous monitoring via a live video stream). Head movement was restricted by a thermoplastic helmet or by a head post. In each session, we performed 10-20 minutes of imaging in the 'spontaneous' condition during which the monkeys performed only occasional spontaneous movements of arms, trunk, and legs, followed by imaging while the animals worked on the 'reaching task' for as long as it took to complete 100 successful trials (median 12 min, inter-quartile range (IQR) 3.5 min). For some of these recordings, TTL pulses from the behavioral task, indicating the occurrence of behavioral events, were recorded on additional channels. The miniscope remained mounted until the end of the session. Imaging and recording parameters were controlled using the Inscopix Data Acquisition Software (IDAS, Inscopix; frame rate, 10 Hz; LED power, 0.6-0.8 mW/mm^2; sensor gain, 7-8X; and electronic focus, 400-900).

Data analysis

Cell identification and trace extraction

Raw calcium imaging recordings, comprised of spontaneous and reaching task conditions, were imported into the IDSP data processing software (Inscopix) for cell identification and trace extraction. The recordings were preprocessed by removing excess pixels, correcting defective pixels using a 3x3 median filter, and performing 4-fold spatial down sampling of each image frame. We then applied a spatial band-pass filter (low and high cut-off points of 0.005 $pixel^{-1}$ and 0.5 $pixel^{-1}$, respectively) and performed rigid translation motion correction with a mean projection image as the global reference frame (to which other frames were aligned). Following that, we used the constrained nonnegative matrix factorization for microendoscopic data (CNMFe) algorithm (Zhou et al., 2018) to extract the calcium transients of individual cells. From the extracted calcium traces, we identified and accepted cells based on imaging metrics such as the cell's spatial footprint, size, and signal-to-noise ratio. Profiles that did not have a somatic appearance (e.g., blood vessels or dendritic segments) or calcium dynamics were rejected from further analysis. On accepted cells, we deconvolved the traces using the "Online Active Set methods for Spike Inference" (OASIS) method (Friedrich et al., 2017; Zhou et al., 2018) to obtain the calcium events per cell. For each recording, we calculated the distance between the cells based on their spatial centroids (X Y coordinates). All data were further analyzed in MATLAB R2023b and R (v 4.4.1). We only report results for the first session in which cells were identified.

Statistical comparisons of calcium activity rates and amplitudes

For each identified cell, we calculated calcium event rates, the coefficient of variation of the inter-event intervals (IEI CV), and the mean amplitude of events during spontaneous and/or reaching task recording conditions. Statistical comparisons, contrasting the calcium event rates in the spontaneous and reaching task conditions in the SMA or M1, were performed using the Wilcoxon signed rank test. We were also able to compare data recorded in M1 and SMA (in monkey U only) in either the spontaneous or task conditions. These comparisons were performed using Wilcoxon rank sum tests. Additionally, we corrected for multiple comparisons using Benjamini-Hochberg false discovery rate (FDR) (Benjamini and Hochberg, 1995). Statistical significance was set at $p < 0.05$.

Alignment to behavioral events

We used TTL pulses generated during the behavioral task to align raw calcium traces to behavioral events, using a custom-written MATLAB algorithm. We were able to analyze data from 7 sessions for monkey Q in the SMA, as well as recordings of single sessions in SMA and M1 for monkey U. For each successful trial, the 3s epoch of raw data starting 1s before target appearance (for monkey Q) or starting 1s before the appearance of the second target (for monkey U) was Z-scored based on data recorded during a control period (a one-second epoch preceding the trial). The mean and standard deviation of Z-scores were then calculated for each cell and all trial conditions (right, center, or left for monkey Q and right or left for monkey U). Results from example sessions are shown in figure 2 and figure S1. Cellular activity was considered as being modulated if the mean calcium activity during the reaching movement (0-1 s after the target appeared for monkey Q and 0-1 s after the second target appeared for monkey U) differed significantly from the mean activity during the 1 s period preceding the target presentation for monkey Q and the appearance of the second target for monkey U. We used Wilcoxon signed rank tests with multiple comparisons corrected at the level of each chamber using FDR. In the SMA of monkey Q, 129 cells were tested across 3 conditions (387 tests); in monkey U's SMA, 14 cells were tested in 2 conditions (28 tests); and in the M1 of monkey U, 6 cells were tested in 2 conditions (12 tests). Cellular activity was considered sensitive to movement direction if only one condition was significant at FDR-corrected p-value <0.05, while non-directionally related neurons were those with a significant response to two or more conditions. The absolute value of the amplitude of change in the z-scored signal between the 1 s preceding the target presentation and the 1 s following the target presentation was also extracted. The magnitude of change in cells showing an increase in activity, and those showing a decrease were compared using a Mann-Whitney rank sum test and comparisons across condition (right, center, or left target) were made with a Kruskal-Wallis test. In all cases, significance was assumed if $p < 0.05$.

Cell coactivation (Jaccard index method)

We examined the synchrony between calcium events using the Jaccard index (implemented using custom R code). Using the deconvolved calcium event data exported from IDPS, we analyzed all sessions from each site (SMA and/or M1). Following (Parker et al., 2018), we first binned the deconvolved calcium events data into 0.2s intervals, then forward-smoothed that data by setting a bin equal to one if a calcium event occurred at any time during the current bin or four bins ahead (a total of 1 s). We then calculated the Jaccard index between all cells (the intersection of the number of forward-smoothed events divided by the union). For each cell pairing, we generated the null distribution of Jaccard indices by randomly circularly shifting the data and recalculating the Jaccard Index 1,000 times. This was repeated 1,000 times. The circular shift preserves the autocorrelation structure of the forward smoothed event data. Next, for each cell pairing, we calculated a normalized version of the Jaccard index by subtracting the mean of the randomly shifted Jaccard indices from the observed Jaccard index and dividing by the standard deviation of the randomly shifted Jaccard indices, which we refer to as the Z-Jaccard. Large positive values of Z-Jaccard indicate cells pairs whose events co-occur substantially more than random circular shifts of the data, which is evidence of synchrony. Large negative values indicate cell pairs whose events co-occur less than expected by chance. We define negative values of the Z-Jaccard as asynchrony. We defined the proportion of cells that were synchronized as the fraction of cell pairs with Z-Jaccard greater than 1.96. For the sessions in which we had both spontaneous and reaching task condition, we compared whether there was a change in the proportion of cells synchronized using a Wilcoxon signed rank test.

We used the centroid information to examine whether there was a relationship between the Z-Jaccard and the distance between cells. A loess smoother (span=1) was used to visualize the relationship between Z-Jaccard and distance.

Determination of precise timed sequences of calcium events

Sequences of calcium events were detected using a custom-written MATLAB algorithm. Sequences of events were defined as the occurrence of two or more calcium spike events (based on the deconvolved data) in a defined temporal order (neuron A -> neuron B -> neuron C) among two or more cells, occurring within a specific time range between the individual events (in this case, 2s). We evaluated sequence occurrences during 10 min segments of recordings made during the spontaneous and arm-reaching task conditions. The algorithm searched for the occurrence rate of all possible combinations of events within a given record and identified those as being significant if they occurred outside of the 95th percentile of shuffled data, using 1,000 circular re-arrangements of events, and if they occurred at least 4 times during the 10 min observation period. Based on the resulting data, we evaluated the number of such sequences, the number of steps of sequential events among cells, the number of sequence repetitions (example depicted in Figure 4A-B), and the spatial distance of sequence members (using the centroid values, see above).

Histology

At the conclusion of the experiments, monkeys were euthanized with an overdose of pentobarbital sodium (100mg/kg, iv). They were then transcardially perfused with oxygenated Ringer's solution, followed by 2 liters of fixative [4% paraformaldehyde, 0.1% glutaraldehyde in phosphate buffer (0.1 M, pH 7.2)]. The fixed brains were then removed from the skull and blocked. The blocks were later cut into 60 µm slices using a vibratome and immunostained for the neuronal marker microtubule-associated protein 2 (MAP2), and for green fluorescent protein (GFP) to examine lens placement and GCaMP6f expression in neuronal cell bodies of projection neurons, respectively. In addition, to confirm the identity of the GCaMP6f expressing neurons, we performed double fluorescent immunolabeling for GABA (as a marker of interneurons). See table 1 for antibody details.

RESULTS

We studied the neuronal activity in SMA and M1 in four macaques using calcium imaging. We used AAVs to express GCaMP6f under control of the Thy1 promoter to target preferentially projection neurons (Feng et al., 2000) in deep cortical layers. Surgical preparations to chronically implant microendoscopic GRIN lenses for optical access to motor cortices and to ensure a stable long-lasting cranial chamber were performed as described in Bollimunta et al. (2021). Out of four subjects, we successfully performed calcium imaging in three SMA sites (monkeys Q, U and F) and two M1 sites (monkeys V and U).

General description of calcium activity

Calcium imaging was done while the animals were sitting in a primate chair and making occasional spontaneous movements ('spontaneous' state), or while they were engaged in a reaching task (monkeys Q and U).

Individual cells and their calcium dynamics were identified using the Constrained Non-negative Matrix Factorization for microendoscopic data (CNMFe) algorithm and validated, based on their activity pattern and morphology (figure 1 A-C; see table S1 for parameters used). The number of identified GCaMP6f-

expressing cells varied across imaging sites and sessions. In the SMA, we identified 129, 61 and 63 cells in monkeys Q, F and U, respectively. In M1, we identified 37 and 23 cells in monkeys U and V, respectively. (table S2). We could track a small portion of cells (18%) across up to three recording sessions.

Calcium events were extracted from the raw calcium traces using the OASIS deconvolution method (see Methods). A comparison of calcium event kinetics revealed region- and task-dependent responses in SMA and M1 neurons. The calcium event rates and the coefficient of variation of the inter-event intervals (IEI CV) did not differ between the spontaneous and reaching task conditions in either cortical region (figure 1D-E). In the SMA, the amplitude of the events was significantly higher in the spontaneous state, compared to the reaching task recordings in Monkey U ($p=0.032$; Wilcoxon signed rank test, corrected for multiple comparisons). In Monkey U, we found that the event rate was higher in M1 than in SMA, both during the spontaneous and reaching task conditions ($p<0.001$ for both, Wilcoxon rank sum test). Similarly, the amplitude of the events was higher for the task in M1, compared to SMA ($p=0.03$, Wilcoxon rank sum test, figure 1D-F).

Calcium trace activity in SMA and M1 shows movement- and movement direction-related responses

To measure task-related encoding of SMA and M1 neurons, we assessed the relationship between calcium activity and a stimulus presentation predictive of motor behavior. In the reaching task, subjects were presented with a single visual cue to prompt a reaching response for a juice reward. In monkey Q's SMA, 34% (43/129) of cells significantly modulated their activity in response to the presentation of the reaching target and the subsequent movement ($p < 0.05$, Wilcoxon signed rank test, corrected for multiple comparisons), as shown in figure 2A, where the average raw calcium traces of 129 cells (obtained across 7 sessions) was aligned to target presentation. In 11/129 cells (9%), the activity was not direction-related, but 32/129 cells (25%), showed larger responses to presentation of the target at a specific position (figure 2B, 2C). The magnitude of the responses did not differ between cells responding with an increase or decrease in firing (Mann-Whitney rank sum test) and the amplitude of the response was similar regardless of the target position (Kruskal-Wallis test; data not shown). Similar results were obtained in the two-target reaching task from monkey U's M1 (figure S1), but no responding cells (0/14) were found in monkey U's SMA in the analyzed session. These data indicate that the calcium imaging method allows identification of a subset of SMA and M1 neurons that are modulated in a direction related manner when presented with a movement-related target in the reaching task.

Cells in SMA and M1 show coactivation

We studied the synchrony between pairs of cells using the Jaccard index, using denoised data. Example sessions are shown for Monkey U in the SMA (figure 3A) and M1 (figure 3B) for spontaneous and task conditions. Pairs of neurons exhibited neural synchrony in both the SMA and M1 during the spontaneous and task conditions (figure 3A-B). The cell pairs exhibiting synchrony were not related to the centroid distances in either SMA or M1 (correlation plot in figure 3A-B). Figure 3C summarizes the proportion of synchronized pairs of cells (Z-Jaccard > 1.96) in the spontaneous and task condition recordings in SMA and M1 for all animals. The proportion of cells that were synchronized tended to decrease during the reaching task in SMA, while the proportion tended to increase in M1. Cell-to-cell synchrony appears to be a reliable feature of SMA and M1 neurons, regardless of task and distance.

Cells in SMA and M1 show sequential activation patterns

We then examined whether ensembles of neurons activate in sequences. We defined a sequence as a series of calcium events involving multiple (≥2) cells, occurring in a specific temporal order with a probability of > 95%, and a minimal repetition rate of ≥ 4 during a 10-minute period in the spontaneous and the reaching task condition. In an example imaging session in monkey Q's SMA, we detected 13 sequences in spontaneous and 17 sequences during the task (figure 4A, top panels). While some of the sequences detected involved the same cells (figure 4A bottom panels), the specific sequences differed (examples highlighted in green in figure 4A, 4B). We also performed the same analysis for sessions in which 20 minutes of spontaneous recording were collected, allowing us to segment the spontaneous segment in two 10-min periods ('spontaneous 1', 'spontaneous 2'). An example from such a recording in monkey Q's SMA is shown in figure 4B. We detected 8, 13 and 9 unique sequences during 'spontaneous 1', 'spontaneous 2' and the reaching task, respectively. The detected sequences differed between all three states, suggesting that the differences between the analyzed segments were not (solely) driven by the behavioral state.

For all imaging sites, and for each recording segment, we calculated the number of sequences (normalized by the number of identified cells), the repetition rate of sequences and the proportion of cells involved in sequences (summarized in figure 4D). We found that these factors varied across conditions and across imaging sites, similar to observations made in monkey Q's SMA.

Finally, we investigated whether cells participating in a sequence were spatially close. Plotting the distribution of distances between pairs of cells that were involved in sequences, as well as the overall distribution of distances between all detected cells showed that there is no preferred spatial relation between cells involved in sequences (figure 4C and S2).

Expression of GCaMP6f and lens localization

Post-mortem histological examination confirmed lens and prism placement in SMA and M1 (figure S3A). The reconstruction of the location of the lens/prism showed that the probes were targeted to the deep cortical layers of the SMA/M1 (right panels in figure S3A). GCaMP6f expression around the imaging sites was revealed by immunoperoxidase against GFP (figure S3B) or by studying the endogenous fluorescence of the calcium sensor (figure S3C). We observed robust GFP expression around the lens/prism for most sites, except in monkey U's SMA, where the GFP expression was sparse. Importantly, many GFP-positive cells showed the morphology of pyramidal cells (i.e., excitatory projection neurons) (Bekkers, 2011). We confirmed that GCaMP6f expression was specific for non-GABAergic neurons by performing a double immunofluorescence assay for GABA and GFP (figure S3D), confirming that GCaMP6f-positivecells are likely to be projection neurons and not interneurons.

DISCUSSION

We examined the activity of projection neurons in deep layers of SMA and M1 of four rhesus macaques, when they were at rest (spontaneous condition) or performing a simple arm reaching task, using calcium imaging techniques. As expected, based on the results of previous electrophysiologic studies, we found that a proportion of SMA and M1 neurons generated calcium transients in relation to arm reaches, and that these responses were often directionally-sensitive. We also identified pairs of projection neurons in SMA and M1 with coincident activity, and dynamically changing sequential activity patterns. Neither coincident nor sequence-related activities differed by spatial distances within the imaged field.

Our study complements the extensive literature on the electrophysiological activity of SMA and M1 neurons in macaques (Nachev et al., 2008), and it builds upon previous studies that have used calcium imaging and miniscopes to examine motor cortex activity in rodents (e.g., (Arroyo et al., 2023; Tombaz et al., 2020)). The calcium imaging method offers unique opportunities to increase our understanding of cortical activity in NHPs, allowing us to image many neurons in deep layers in M1 and SMA. As an important distinction to the previous electrophysiologic studies in rhesus monkeys, by combining a genetic strategy (use of the Thy1 promoter which targets preferentially projection neurons (Feng et al., 2000)) and placing the GRIN lenses in deep cortical layers, we selectively monitored cortico-fugal neurons.

We compared calcium activity from the spontaneous to the reaching task condition in individually identified neurons that were reliably tracked within a session. We found that neither the rate nor the variability of calcium events differed significantly between the two conditions, perhaps indicating that the information coded by these parameters is not indicative of the behavioral state of the animal. However, a previous microendoscopic calcium imaging study in the M1 of marmosets reported an increase in calcium event rates from rest to movement (Kondo et al., 2018) a difference that could be due to the more complex tasks the marmosets were engaged in (reaching for food pellets or climbing ladders).

We found that calcium event rates were, in general, higher in M1 neurons than in SMA neurons, which differs from electrophysiology studies which report similar firing rates in both regions (Chen et al., 1991). The difference may be partially explained by the fact that the electrophysiologic measurements were not specific for corticofugal neurons. In addition, the two techniques detect different neuronal activity patterns: while electrophysiologic recordings identify both single spikes and bursts of firing, calcium imaging is more sensitive to bursts of activity (Chen et al., 2013). Our result may therefore reflect a difference in resting firing patterns between M1 and SMA rather than a different overall activity of neurons in these regions.

In our study, the calcium event rate was about 10-fold higher than previously reported in the premotor cortex of rhesus macaques (Bollimunta et al., 2021). The rate of calcium events we detected was also different from that reported in the M1 of marmosets (Kondo et al., 2018). These discrepancies are likely not only related to species differences (in the case of the marmosets), but also a direct result of the definition of 'calcium events': our calculation of the event rate is based on the detection of such events with a deconvolution method, unlike the study of Bollimunta et al. (2021).

In a subpopulation of SMA and M1 neurons the calcium activity was related to arm reaches, and some neurons showed directional sensitivity, as previously observed with electrophysiological recordings (Chen et al., 1991; Nachev et al., 2008; Tanji and Mushiake, 1996). Similar results were reported in another study using microscopic calcium imaging in the M1 of marmosets (Kondo et al., 2018). Thus, even though the time resolution of calcium transients is orders of magnitude lower than electrophysiological recordings, the calcium imaging method can detect basic functional parameters of these cortical regions.

Microendoscopic calcium imaging can simultaneously monitor many cells in a relatively large area of cortex, allowing analysis of simultaneous and sequential activation of neurons. In SMA and M1 we found pairs of cells that that were coactive, unrelated to their spatial proximity (within the confines of the evaluated imaging field). Our results in the macaque motor cortices differ from the findings of Parker et al, who reported coactivation in spatially close groups of striatal medium spiny neurons in rodents (Parker et al., 2018), likely due to different structural organization across brain regions.

In a related analysis, we found that the activity of neurons in M1 and SMA can form recurring sequential patterns, involving multiple cells. Similarly to the findings of the coactivation analysis, the distance between neurons did not predict their involvement in sequences. The sequences were not stable over time, and not specifically dependent on the behavioral context of the recordings, as variations of patterns were also seen when comparing different segments of recordings done in the spontaneous condition. We could not derive a true estimate of the variability of the statistically identified sequences because the low calcium event rates preclude an examination of these sequences in short time intervals. Given that the identified sequence interactions occurred over relatively long periods, they are not likely to be the product of local neuronal interactions but may represent long-range network activities.

As far as we know, this is the first report of the use of calcium imaging to examine neuronal sequential activation patterns. Sequential activation patterns of neurons have been studied before, e.g., in electrophysiologic and calcium imaging studies of bird song (e.g., (Mackevicius et al., 2023; Okubo et al., 2015) where sequential patterns can be traced to precise vocal patterns. As mentioned, we have not found clear links of sequence patterns to behavior in our animals, but it is possible that the detected sequences could be related to functional processes that were not directly assessed in our study, such as attentional or motivational states.

The calcium imaging technique has some important limitations. The temporal resolution of the calcium transient imaging procedure is much lower than that of electrophysiological recordings, limiting the analysis of neuronal events that occur at faster time scales. One reported advantage of the calcium imaging technique using miniscopes is the ability to track the same cells across days (Sheintuch et al., 2017), based on the spatial stability of fluorescence and surrounding tissue landmarks within the imaged field. However, in our study we were not able to routinely track neurons across multiple sessions. This issue was also reported in studies conducting calcium imaging in the M1 of rats (Boschen et al., 2024). Several factors may impact the ability to longitudinally track calcium transients in the same cells. One factor could be that the expression of GCaMp6f is not stable, but this seems unlikely as we noted robust expression of the calcium sensor in our postmortem studies. Alternatively, changes in the field of view, due to movement of the brain tissue in relation to the GRIN lenses, may interfere with longitudinal recordings. It is conceivable that this may differ between animal species, or even between brain regions within the same animal.

The sparse GCaMp6f expression in monkey U's SMA may explain the low number of cells imaged in this animal. However, the GCaMP6f expression levels observed post-mortem in monkeys F and V, and in monkey U's M1 were much higher, but the number of cells imaged *in vivo* were also found to be comparatively low. Overall, the total number of neurons imaged per session in our studies ranged from 23 to 129 (Table S4), which contrasts to a reported average of 90 cells in the rat M1 (Boschen et al., 2024). This difference may reflect the fact that the neuron density is lower in the primate M1 compared to that of the rodent M1 (Heffernan et al., 2024; Herculano-Houzel, 2014).

In summary, we used microendoscopic calcium imaging to study groups of neurons in the SMA and M1 in rhesus macaques, across behavioral states. Our study sets the stage for use of this method to examine calcium dynamics in groups of cells in the primate motor cortices in more complex and controlled behavioral tasks, to compare patterns of activity among cells in disease states, such as parkinsonism (Blesa et al., 2018) , and to study neuronal responses to acute or chronic treatments in these models. Finally, given the ongoing development of enhancer sequences that can be used in AAVs or other viral vectors

(Vormstein-Schneider et al., 2020), it may soon be possible to expand this technique to track the activity of other neuronal subtypes (e.g., subtypes of cortical inhibitory interneurons, or specific cortical projection neurons).

ACKNOWLEDGMENTS AND FUNDING SOURCES

We are grateful to Wendy Williamson Coyne for assistance during surgeries, and to Susan Jenkins, DeErra Locklin and Charlotte Armstrong for technical help. Some of the surgeries described in this study were conducted in collaboration with the Emory Translational Neuroscience Core, which is supported by the Department of Neurosurgery, Emory University School of Medicine.

This research was funded by Aligning Science Across Parkinson's [ASAP-020572] through the Michael J. Fox Foundation for Parkinson's Research (MJFF) and by NIH P51-OD011132 (Emory National Primate Research Center).

AUTHORS CONTRIBUTIONS

Conceptualization, J.J.N, T.W., A.G.; Methodology, J.J.N., W.Y., J. D., T.W., A.G.; Software, B.R., A.D., T.W.; Investigation, A.C.M, D.P., A.G.; Formal Analysis, A.C.M., D.P., A.D., B.R., T.W.; Writing – Original Draft, A.C.M, D.P., A.G.; Writing – Review & Editing, A.D., B.R., J.J.N., W.Y., T.W., Visualization, A.C.M., D.P., A.D., B.R., T.W., A.G.; Supervision, T.W., A.G., Funding Acquisition, T.W., A.G.

DECLARATION OF INTERESTS

W.Y., J.D., and J.J.N. are paid employees of Inscopix, Inc. The remaining authors declare no competing interests.

SUPLEMENTAL INFORMATION

Tables S1-S4 and Figures S1-S2.

FIGURES

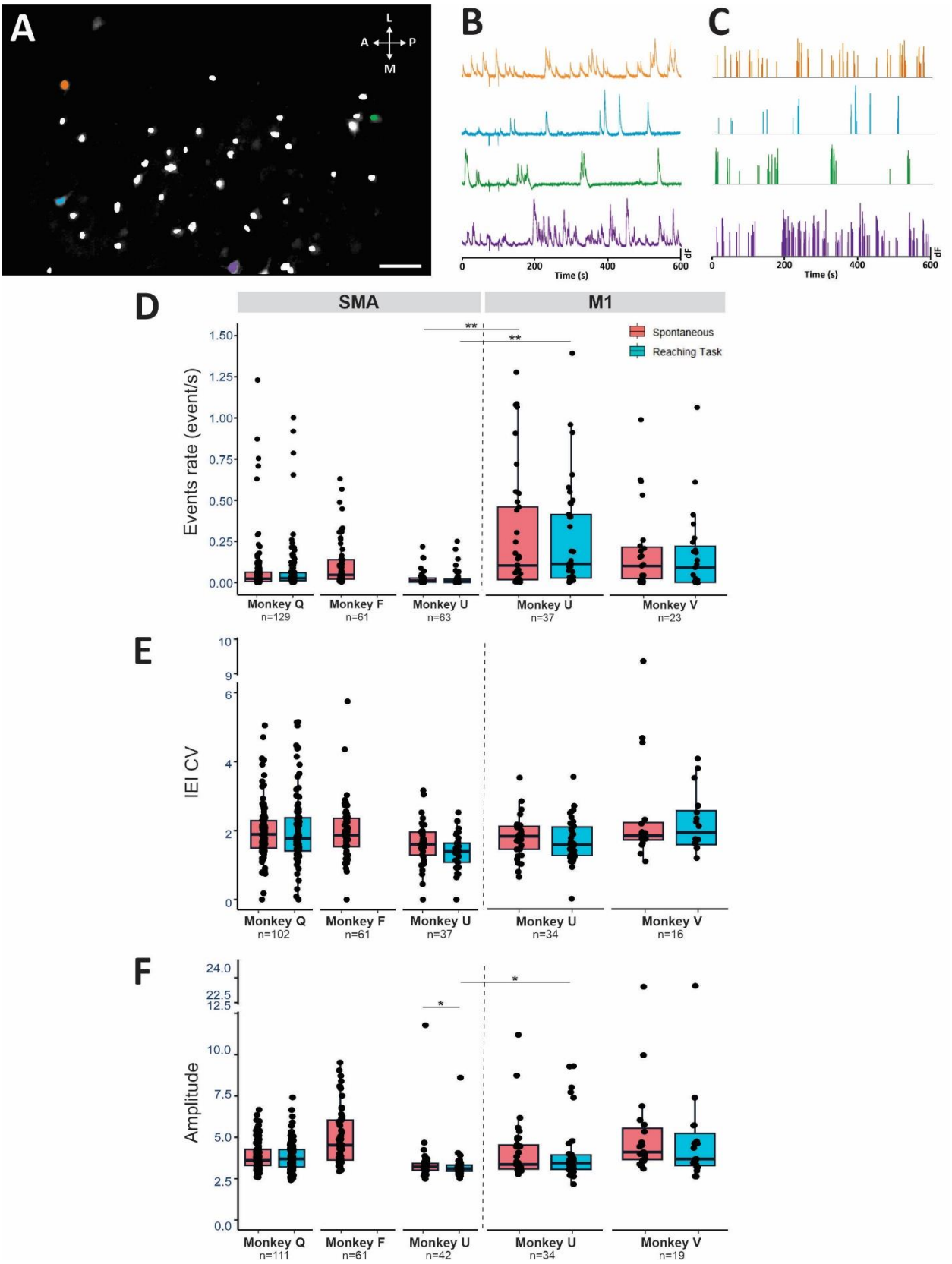
A
L
A
P
M
B
C
0
200
400
600
Time (s)
dF
D
SMA
M1
Spontaneous
Reaching Task
Events rate (event/s)
1.50
1.25
1.00
0.75
0.50
0.25
0.00
**
**
Monkey Q
n=129
Monkey F
n=61
Monkey U
n=63
Monkey U
n=37
Monkey V
n=23
E
IEI CV
10
9
6
4
2
0
Monkey Q
n=102
Monkey F
n=61
Monkey U
n=37
Monkey U
n=34
Monkey V
n=16
F
Amplitude
24.0
22.5
12.5
10.0
7.5
5.0
2.5
0.0
*
*
Monkey Q
n=111
Monkey F
n=61
Monkey U
n=42
Monkey U
n=34
Monkey V
n=19

Figure 1: Steps of analysis and general description of cell activity A: Maximal intensity of GCaMP6f fluorescence in the SMA during a single example session (monkey Q), overlapped on the cell map (white) extracted using CNMF-E. Orange, blue, green, and purple symbols mark the example cells shown in B and C. Scale bar: 100 µm. **B:** Raw traces of calcium transients (dF, peak-normalized) during spontaneous activity. **C:** Calcium events deconvolved from the calcium traces in B. **D, E, F:** Box plots summarizing the event rate (events/s), inter-event interval coefficient of variation (IEI CV) and amplitude of events detected across all sessions in the SMA (left) and M1 (right) in the spontaneous condition (red) and during the arm reaching task (blue). The horizontal bar in each box indicates the median, each circle indicates the median value for a cell. * $p < 0.05$, ** $p < 0.001$; Wilcoxon signed rank tests corrected for multiple comparisons using the false discovery rate (FDR).

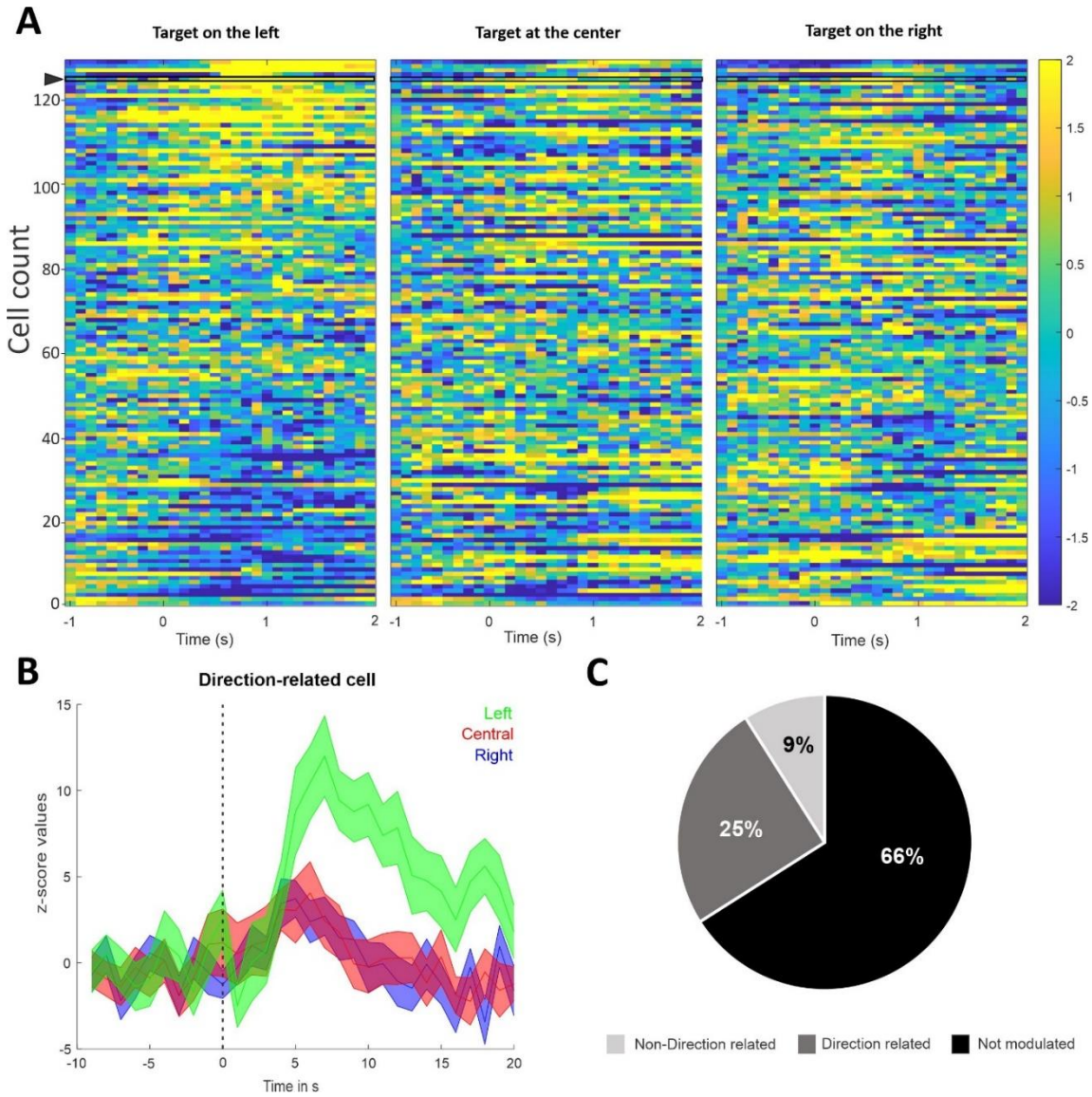

Figure 2: Different responses of SMA cells to target laterality. A: Heat maps of the Z-scored raw calcium traces for each cell in the population, aligned on the appearance of the target on the right, center or left of the screen during the single-target reaching task in monkey Q (n=129 cells, average of 30 trials/conditions). In the left panel, the cells have been sorted, based on their directional selectivity. On the middle and right panel, cells are sorted in the same order as left panel. **B:** Example of a direction-related cell, indicated by the arrow in A, with a significantly higher increase of activity on the target's presentation on the left. The cell's activity is aligned on the appearance of the target marked by the vertical dash line. Colored curves represent the average Z-score activity ± SD, separately for movements to left (green, p=0.03), central (red p=0.92) and right (blue, p=0.43) targets. **C:** Pie chart representing the proportion of cells that were not modulated, direction-related or non-direction related (black, dark grey light grey respectively). Significance evaluated with an FDR-corrected Wilcoxon signed rank test with $p<0.05$.

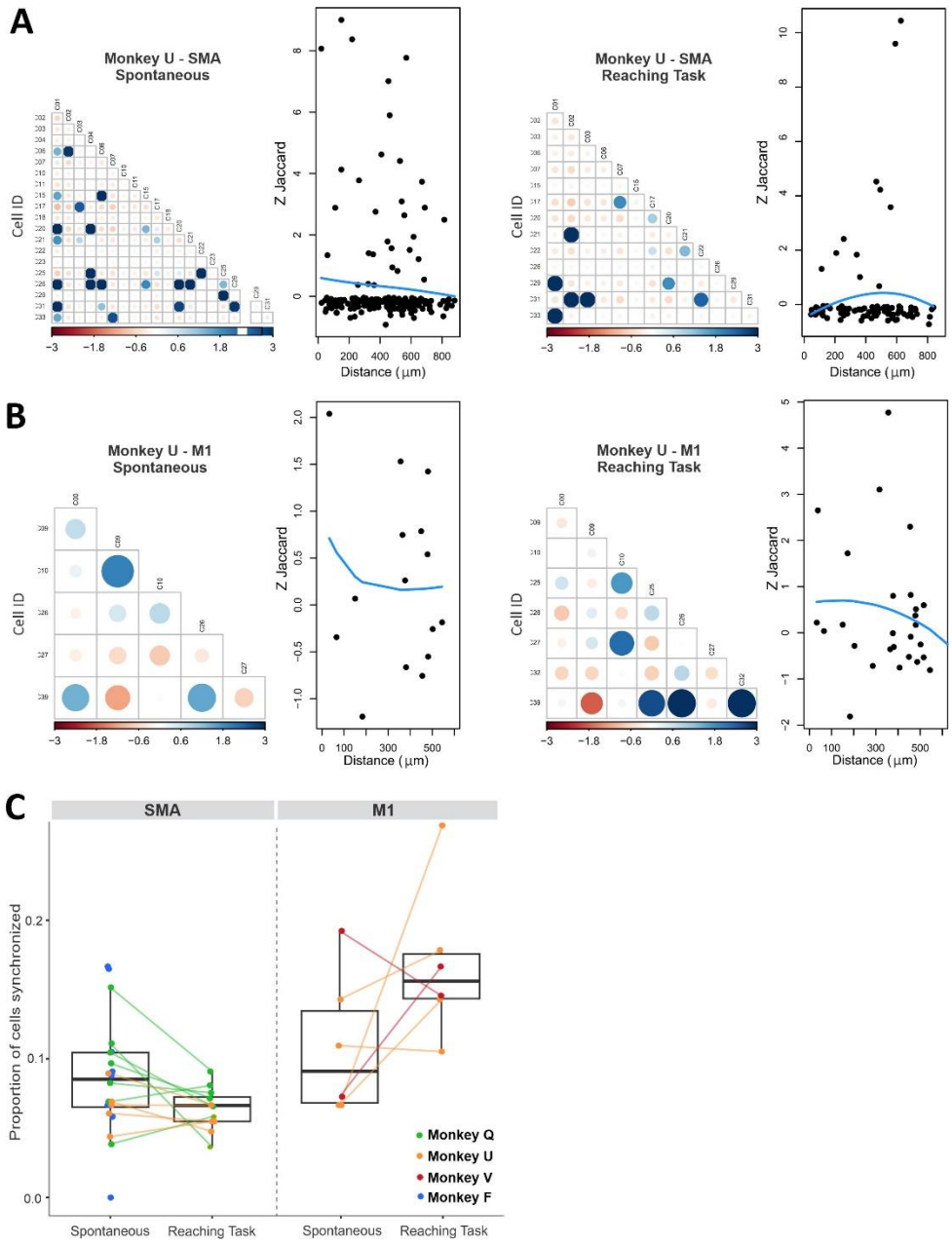

Figure 3: Coactivation between cells events in both SMA and M1. A: Coactivation plots based on recordings made during the spontaneous and the task conditions in SMA in one example session from monkey U. Circles represent normalized Jaccard index (Z-Jaccard) for each cell pairing. Large/dark blue circles indicate positive values of Z-Jaccard and large/dark red circles indicate negative values of Z-Jaccard. On the right of each coactivation plot, we show the correlation plots between Z-Jaccard index and distance between the centroids of the cells. **B:** Example session from monkey U in M1. Same legend as panel A. **C:** Box plot summarizing the proportion of cells synchronized during spontaneous and task conditions in SMA and M1. The horizontal bars represent the median value across all animals (monkeys Q, U, V and F in green, orange, red, and blue respectively). Each dot represents the average value for one session. Spontaneous and task values from the same session are connected by a line.

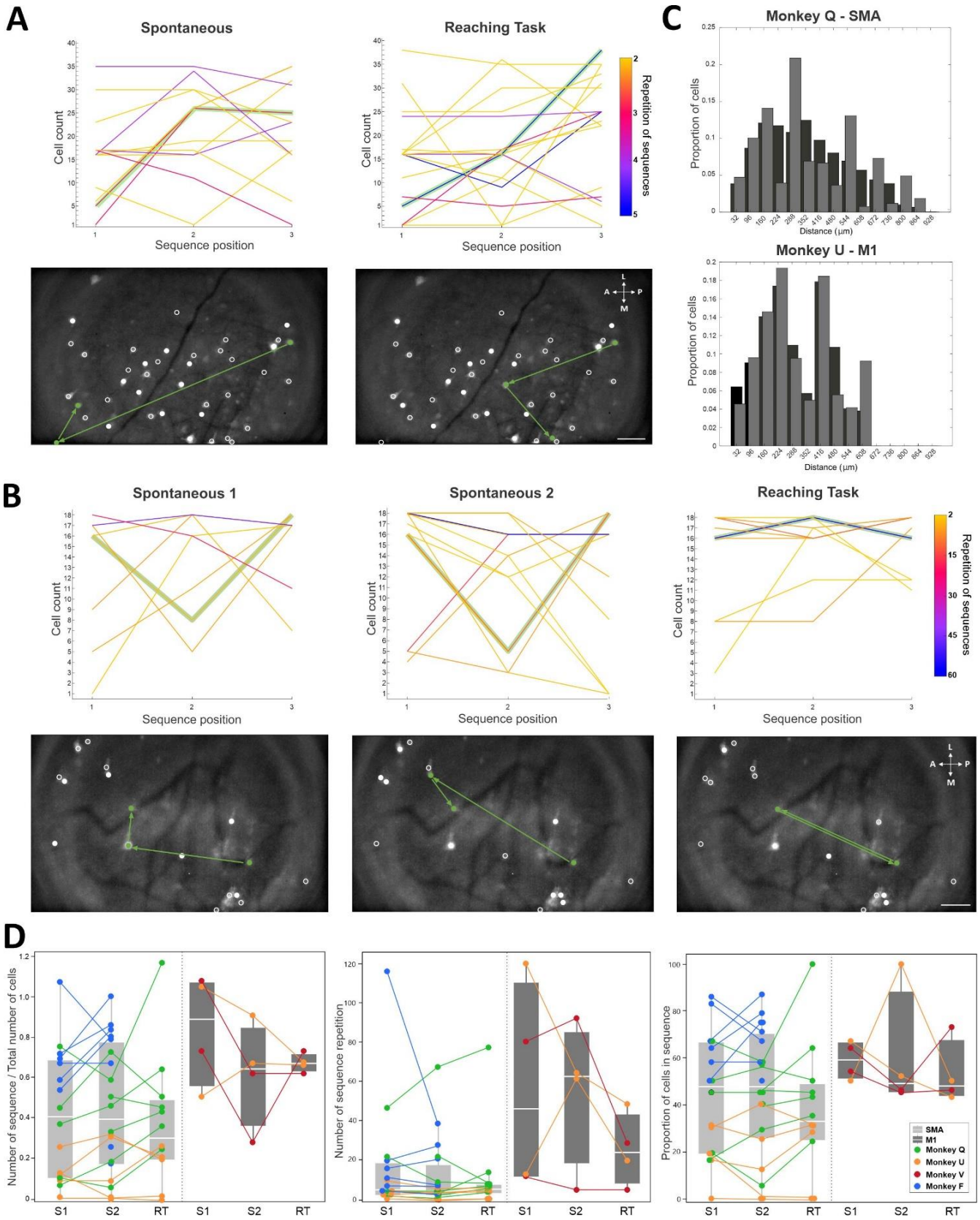
A
Spontaneous
Reaching Task
Cell count
Sequence position
Repetition of sequences
C
Monkey Q - SMA
Monkey U - M1
Proportion of cells
Distance (µm)
B
Spontaneous 1
Spontaneous 2
Reaching Task
D
Number of sequence / Total number of cells
Number of sequence repetition
Proportion of cells in sequence
S1
S2
RT
SMA
M1
Monkey Q
Monkey U
Monkey V
Monkey F

Figure 4: Repeating sequences of calcium events involving several neurons in the spontaneous condition and during the reaching task. A: Top row, depiction of sequences found across 40 cells in an example session in monkey Q's SMA, during spontaneous and reaching task conditions. The x-axis indicates the position of the cell within a sequence. The line thickness indicates the number of repetitions of the sequences. An example sequence starting with cell #5 is highlighted in green for the spontaneous and for the task condition. Below each graph we show the maximal GCaMP6f fluorescence intensity overlapped with the map of cells detected (white circles). The green circles illustrate the three cells involved in the sequence and the green arrows indicate the temporal order. Although cell #5 initiates the sequence in both examples, it is followed by different cells in the spontaneous and reaching task. Scale bar: 100 µm. **B:** Sequences found across 18 cells in a different session in monkey Q's SMA, during two 10 min segments of the spontaneous conditions ('spontaneous 1', 'spontaneous 2') and during the reaching task. Same conventions as described for figure 4A. **C:** Spatial distribution of cells involved in sequences. Black bars indicate the distribution of the centroids of all the cells recorded across all sessions in the spontaneous condition in monkey Q SMA (top) and monkey U M1 (bottom). Grey bars indicate the distribution of the centroids of the cells involved in sequences. Note overlap of the distributions, indicating that cells involved in sequences were not clustered, but spread across the field of view. **D:** Box plots representing normalized number of sequences, number of repetition and proportion of cell in sequence across monkeys in SMA (light grey) and M1 (dark grey). Each dot represents median values for a session. Monkey Q (green), U (yellow) F (blue) and V (red). Data is binned in 10 min of recording in spontaneous (S1 and S2) and during the reaching task (RT).

REFERENCES

Alexander, G.E., and Crutcher, M.D. (1990). Functional architecture of basal ganglia circuits: neural substrates of parallel processing. Trends in neurosciences *13*, 266-271.

Alexander, G.E., DeLong, M.R., and Strick, P.L. (1986). Parallel organization of functionally segregated circuits linking basal ganglia and cortex. Annu Rev Neurosci *9*, 357-381.

Arroyo, S., Barati, S., Kim, K., Aparicio, F., and Ganguly, K. (2023). Emergence of preparatory dynamics in VIP interneurons during motor learning. Cell Reports *42*.

Bekkers, J.M. (2011). Pyramidal neurons. Curr Biol *21*, R975.

Benjamini, Y., and Hochberg, Y. (1995). Controlling the False Discovery Rate - a Practical and Powerful Approach to Multiple Testing. J R Stat Soc B *57*, 289-300.

Blesa, J., Trigo-Damas, I., Del Rey, N.L., and Obeso, J.A. (2018). The use of nonhuman primate models to understand processes in Parkinson's disease. J Neural Transm (Vienna) *125*, 325-335.

Bollimunta, A., Santacruz, S.R., Eaton, R.W., Xu, P.S., Morrison, J.H., Moxon, K.A., Carmena, J.M., and Nassi, J.J. (2021). Head-mounted microendoscopic calcium imaging in dorsal premotor cortex of behaving rhesus macaque. Cell Rep *35*, 109239.

Boschen, S.L., Seethaler, J., Wang, S., Lujan, W.D., Silvernail, J.L., Carter, R.E., Chang, S.Y., and Lujan, J.L. (2024). Midbrain dopaminergic degeneration differentially modulates primary motor cortex activity and motor behavior in hemi-parkinsonian rats. Res Sq.

Chen, D.F., Hyland, B., Maier, V., Palmeri, A., and Wiesendanger, M. (1991). Comparison of neural activity in the supplementary motor area and in the primary motor cortex in monkeys. Somatosens Mot Res *8*, 27-44.

Chen, T.W., Wardill, T.J., Sun, Y., Pulver, S.R., Renninger, S.L., Baohan, A., Schreiter, E.R., Kerr, R.A., Orger, M.B., Jayaraman, V.*, et al.* (2013). Ultrasensitive fluorescent proteins for imaging neuronal activity. Nature *499*, 295-300.

Drucker, C.B., Carlson, M.L., Toda, K., DeWind, N.K., and Platt, M.L. (2015). Non-invasive primate head restraint using thermoplastic masks. J Neurosci Methods *253*, 90-100.

Feng, G., Mellor, R.H., Bernstein, M., Keller-Peck, C., Nguyen, Q.T., Wallace, M., Nerbonne, J.M., Lichtman, J.W., and Sanes, J.R. (2000). Imaging neuronal subsets in transgenic mice expressing multiple spectral variants of GFP. Neuron *28*, 41-51.

Friedrich, J., Zhou, P., and Paninski, L. (2017). Fast online deconvolution of calcium imaging data. PLOS Computational Biology *13*, e1005423.

Heffernan, K.S., Martinez, I., Jaeger, D., Khakh, B., Smith, Y., and Galvan, A. (2024). Scaled complexity of mammalian astrocytes: insights from mouse and macaque. J Comp Neurol. *532,* e25665.

Herculano-Houzel, S. (2014). The glia/neuron ratio: how it varies uniformly across brain structures and species and what that means for brain physiology and evolution. Glia *62*, 1377-1391.

Kondo, T., Saito, R., Otaka, M., Yoshino-Saito, K., Yamanaka, A., Yamamori, T., Watakabe, A., Mizukami, H., Schnitzer, M.J., Tanaka, K.F*., et al.* (2018). Calcium Transient Dynamics of Neural Ensembles in the Primary Motor Cortex of Naturally Behaving Monkeys. Cell Rep *24*, 2191-2195 e2194.

Mackevicius, E.L., Gu, S., Denisenko, N.I., and Fee, M.S. (2023). Self-organization of songbird neural sequences during social isolation. Elife *12*.

McFarland, N.R., and Haber, S.N. (2001). Organization of thalamostriatal terminals from the ventral motor nuclei in the macaque. J Comp Neurol *429*, 321-336.

Middleton, F.A., and Strick, P.L. (2000). Basal ganglia and cerebellar loops: motor and cognitive circuits. Brain Res Brain Res Rev *31*, 236-250.

Nachev, P., Kennard, C., and Husain, M. (2008). Functional role of the supplementary and pre-supplementary motor areas. Nat Rev Neurosci *9*, 856-869.

Oguchi, M., Jiasen, J., Yoshioka, T.W., Tanaka, Y.R., Inoue, K., Takada, M., Kikusui, T., Nomoto, K., and Sakagami, M. (2021). Microendoscopic calcium imaging of the primary visual cortex of behaving macaques. Sci Rep *11*, 17021.

Okubo, T.S., Mackevicius, E.L., Payne, H.L., Lynch, G.F., and Fee, M.S. (2015). Growth and splitting of neural sequences in songbird vocal development. Nature *528*, 352-357.

Parker, J.G., Marshall, J.D., Ahanonu, B., Wu, Y.W., Kim, T.H., Grewe, B.F., Zhang, Y., Li, J.Z., Ding, J.B., Ehlers, M.D*., et al.* (2018). Diametric neural ensemble dynamics in parkinsonian and dyskinetic states. Nature *557*, 177-182.

Paxinos, G., Huang, X.F., and Toga, A.W. (2000). The Rhesus Monkey Brain in Stereotaxic Coordinates (San Diego, CA: Academic Press).

Picard, N., and Strick, P.L. (1996). Motor areas of the medial wall: a review of their location and functional activation. Cereb Cortex *6*, 342-353.

Pollmann, E.H., Yin, H., Uguz, I., Dubey, A., Wingel, K.E., Choi, J.S., Moazeni, S., Gilhotra, Y., Pavlovsky, V.A., Banees, A*., et al.* (2023). Subdural CMOS optical probe (SCOPe) for bidirectional neural interfacing. bioRxiv, 2023.2002.2007.527500.

Sheintuch, L., Rubin, A., Brande-Eilat, N., Geva, N., Sadeh, N., Pinchasof, O., and Ziv, Y. (2017). Tracking the Same Neurons across Multiple Days in Ca²⁺ Imaging Data. Cell Reports *21*, 1102-1115.

Strick, P.L., Dum, R.P., and Rathelot, J.A. (2021). The Cortical Motor Areas and the Emergence of Motor Skills: A Neuroanatomical Perspective. Annu Rev Neurosci *44*, 425-447.

Tanji, J., and Mushiake, H. (1996). Comparison of neuronal activity in the supplementary motor area and primary motor cortex. Brain Res Cogn Brain Res *3*, 143-150.

Tombaz, T., Dunn, B.A., Hovde, K., Cubero, R.J., Mimica, B., Mamidanna, P., Roudi, Y., and Whitlock, J.R. (2020). Action representation in the mouse parieto-frontal network. Sci Rep *10*, 5559.

Vormstein-Schneider, D., Lin, J.D., Pelkey, K.A., Chittajallu, R., Guo, B., Arias-Garcia, M.A., Allaway, K., Sakopoulos, S., Schneider, G., Stevenson, O.*, et al.* (2020). Viral manipulation of functionally distinct interneurons in mice, non-human primates and humans. Nat Neurosci.

Zhou, P., Resendez, S.L., Rodriguez-Romaguera, J., Jimenez, J.C., Neufeld, S.Q., Giovannucci, A., Friedrich, J., Pnevmatikakis, E.A., Stuber, G.D., Hen, R.*, et al.* (2018). Efficient and accurate extraction of in vivo calcium signals from microendoscopic video data. Elife *7*.

SUPPLEMENTAL INFORMATION

Preprocess			Spatial Filter		Motion Correction		
Spatial Downsampling	**Fix defective pixels (Yes/No)**	**Trim early frames (Yes/No)**	**Low**	**High**	**Global ref. frame**	**Use ROI (Yes/No)**	**Preserve input dimension (Yes/No)**
4	Yes	Yes	0.005	0.5	Mean Image	Yes	Yes
CNMFe Cell Identification					**OASIS Deconvolution**		
Avg. Cell Diameter (pixels)	**Min. Pixel correlation**	**Min. Peak to Noise ratio**	**Guaussian filter width (pixels)**	**Merging threshold**	**Spike SNR Threshold**		
7-20	0.75 - 0.80	8-10	8-20	0.3	2.5		

Table S1: Parameters for cell identification and deconvolution.

Animal ID	Structure	Total imaging period(weeks)	Number of sessions	Total cells identified at least in one session	Cells identified in more than one session
Q	SMA	21	7	129	23
F	SMA	9	6	61	17
U	SMA	14	5	63	15
U	M1	14	4	37	6
V	M1	14	2	23	1

Table S2: Number of sessions and cells identified per imaging site.

REAGENT OR RESOURCE	SOURCE	IDENTIFIER
Plasmids		
pAAV TREGCaMP6f	Addgene	Cat # 97410
pAAV ThyStTA	Addgene	Cat # 97411
Viral vectors		
AAV5-TRE-GCAMP6f	Vigene Biosciences	n/a
AAV5-ThyStTA	Vigene Biosciences	n/a
Antibodies		
Chicken anti-GFP (immunofluorescence)	Millipore	Cat # 06-896 RRID: AB_310288
Rabbit anti-GFP (immunoperoxidase)	Thermo Fisher (Invitrogen)	Cat # A-11122 RRID: AB_221569
Mouse anti-MAP2	Millipore	Cat # MAB3418 RRID: AB_11212326
Rabbit anti-GABA	Sigma	Cat # A2052 RRID: AB_477652
Biotinylated goat anti-rabbit	Vector	Cat # BA1000 RRID: AB_2313606
Biotinylated goat anti-mouse	Vector	Cat # BA9200 RRID: AB_2336171
Donkey anti-chicken (Fluorescein)	Jackson Lab	Cat # 703-095-155 RRID:AB_2340356
Donkey anti-rabbit (Rhodamine red-X)	Jackson Lab	Cat # 711-295-152 RRID:AB_2340613
PROTOCOLS		
Surgery to inject viral vectors and implant GRIN lenses	dx.doi.org/10.17504/protocols.io.e6nvw15w2lmk/v1	
Miniscope calcium imaging data acquisition of cortical activity	dx.doi.org/10.17504/protocols.io.14egn612pl5d/v1	
Immunoperoxidase staining	dx.doi.org/10.17504/protocols.io.14egn2b6mg5d/v1	

Table S3: Key Resources

Site	No. of injection tracks	Number of deposits	Deposit dorso-ventral location (mm)	Volume delivered per deposit (μl)
Monkey Q SMA	1	3	7, 6.5, 5.5	2.3, 1.8, 1.4
Monkey Q M1	1	2	4, 3	2, 1.3
Monkey U SMA	1	3	4.9, 4.4, 3.4	2, 1.5, 1.5
Monkey U M1	1	2	3.7, 2.7	1.5, 1.5
Monky V SMA	1	3	5.8, 5.3, 4.3	2, 1.5, 1.5
Monkey V M1	1	2	5.3, 4.3	1.5, 1.5
Monkey F SMA	1	4	5.5, 5, 4.5, 4	1.6, 1.6, 3, 1.6
Monky F M1	1	4	6.7, 6.2, 5.2, 4.7	1.6, 1.6, 1.6, 1.6

Table S4: Details of AAV injections

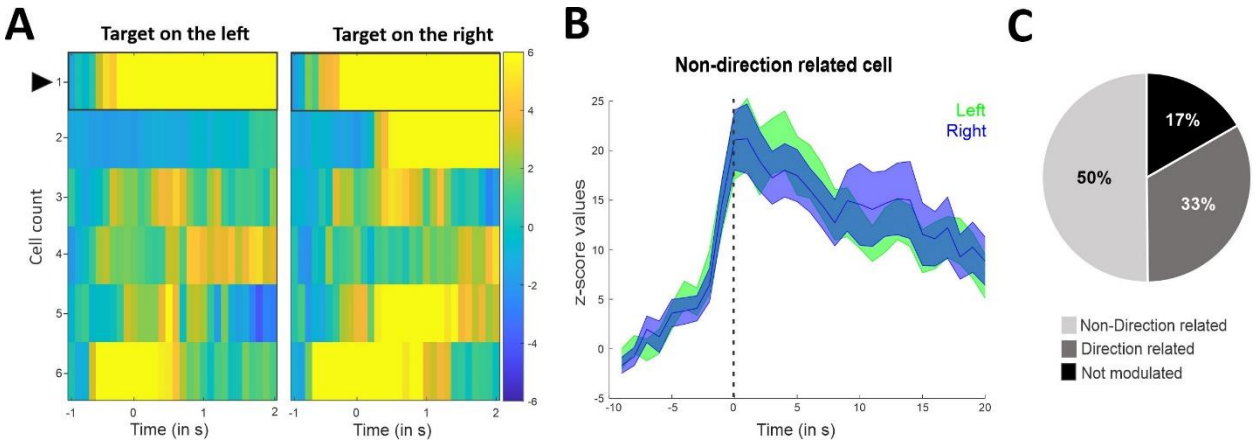

Figure S1: Different responses of M1 cells to target laterality. A: Heat maps of the Z-scored raw calcium traces of each cell in an example session in M1, aligned on the appearance of the right or left target during the two- target reaching task in monkey U (n=6 cells, 50 trials/condition). On the left panel, the cells have been sorted on their selectivity. On the right panel, cells are sorted in the same order as panel left. **B:** Example of non-direction related cell, indicated by the arrow in A, with a significant increase toward both right and left targets ($p<0.01$ target left, $p<0.01$ target right, FDR-corrected Wilcoxon signed rank with $p<0.05$). The cell's activity is aligned on the appearance of the second target marked by the vertical dash line. Colored curves represent the average z-score activity ± SD separately for left (green), and right (blue) targets. **C:** Pie chart representing the proportion of cells that are not modulated (black), direction related (dark grey) and non-direction related (light grey).

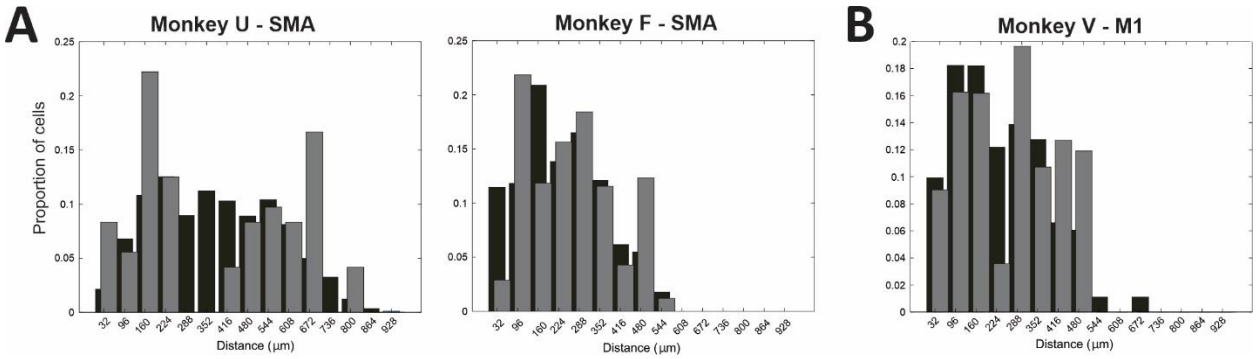

Figure S2: Spatial distribution of cells involved in sequences and sequence parameters A: Black bars indicate the distribution of the centroids of all cells recorded across all sessions in the spontaneous condition for monkey U and F in SMA, monkey V in M1. Grey bars indicate the distribution of the centroids of the cells involved in sequences. Note almost complete overlap of the distributions, indicating that cells involved in sequences were not clustered, but spread across the field of view.

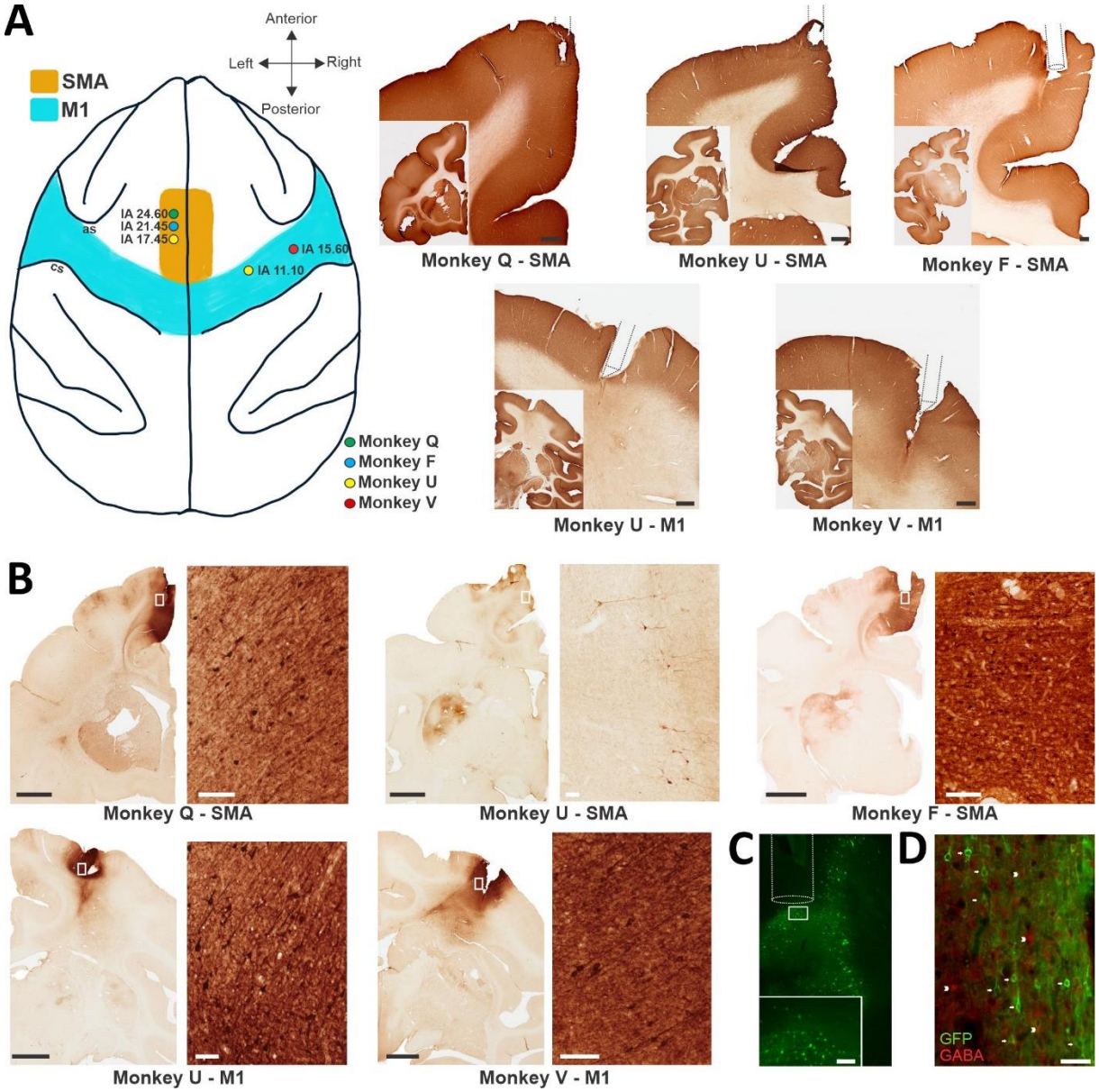

Figure S3: GCaMP6f expression and lens location in SMA and M1. A: This diagram indicates the location of GRIN lenses, based on post-mortem verification in SMA and M1 for monkeys Q (green dot), F (blue dot), U (yellow dots) and V (red dot) with the corresponding interaural coordinates (based on the atlas by Paxinos et al 2000). Abbreviations: as, arcuate sulcus; cs, central sulcus. Right: Reconstructions of the lens placement in SMA (top row) and prism placement in M1 (bottom row) in MAP-2 stained brain sections. Black scale bars, 1 mm. **B:** GFP immunoperoxidase (to reveal GCaMP6f expression) in SMA and and M1. The white rectangles are shown at higher magnification on the right. Black scale bars, 4 mm; white scale bars, 100 µm. **C:** Endogenous green fluorescence of GCaMP6f in a section adjacent to those shown in A and B for monkey Q. Reconstruction of lens placement (white line), lens diameter is 1 mm. The white rectangle is shown at higher higher magnification on the right. White scale bar, 100 µm. **D:** Double immunofluorescence for GFP and GABA in the M1 of monkey U. Green indicates GFP (GCaMp6f)-positive cells, some indicated by arrows). Red indicates GABA-positive cells (some indicated by arrowheads). No overlap of the signals was observed, suggesting that GCaMp6f-expressing cells are not GABAergic interneurons. White scale bar, 50 µm.